

CONTENTS

I. Introduction	2
II. Curvaton model	3
III. PBH production	5
IV. Constraints of the secondary gravitational wave	7
V. Results	7
A. Classical dynamics of the complex scalar	7
B. The perturbation of the curvaton	8
C. Curvature power spectrum and PBH production	9
D. Secondary gravitational wave	11
E. Constraint of isocurvature	11
VI. Conclusion	11
Acknowledgements	12
A. Equation of motion of the curvaton	12
B. The curvaton energy ratio	13
References	13

I. INTRODUCTION

Since the first gravitational wave event was discovered in 2015, several binary black hole (BBH) merger events have been observed by LIGO-Virgo collaboration [1–6]. Many of these black holes (BHs) have masses around $30M_{\odot}$ ($= 60 \times 10^{30}$ kg). It seems difficult to produce such heavy BHs from an evolution of stars with the usual metalicity [7–9]. One possible scenario is BH formation from the first Population III stars [10]. Primordial black hole (PBH) scenario is another promising solution to the origin of the BBH mergers [11–15]. PBHs can be produced by gravitational collapse of an overdense region in the radiation-dominated era or the early matter-dominated era [16–18].

PBHs are also interesting as dark matter (DM) candidate. The microlensing observations give stringent constraints on the DM PBH mass and in particular, the observation with Subaru Hyper Supreme-Cam (HSC) almost closed the DM mass window [19–22]. However, recently it has been found that the so-called "wave effect" ¹ weakens the lensing effect and PBHs with mass 10^{-13} – $10^{-10}M_{\odot}$ can still account for all DM of the universe.

Since extensive researches put the severe constraints on the mass distribution of PBHs (see Fig.3,4,5), a PBH production mechanism should have a peak-like mass distribution to explain the LIGO events or PBH-DM scenario successfully. PBH production also requires the large amplitude of density perturbations in the small scales, 10^{-5} Mpc for LIGO PBHs and 10^{-12} Mpc for DM PBHs. Since cosmic microwave background (CMB) and large scale structure (LSS) observations show that the spectrum of the curvature perturbations on large scales $1 \text{ Mpc} \sim 10^3 \text{ Mpc}$ is nearly scale invariant and its amplitude is small, the small-scale perturbations responsible for PBHs can hardly be produced in simple single-field inflation models and may require a different mechanism, for example, multi-fields inflation [23], double-inflation [24], curvaton dynamics [25, 26].

In this paper we investigated an axion-like curvaton model [26–28] with an inflaton-coupling term. Our model controls large-scale perturbations of the curvaton with the inflaton-coupling in the same way as the inflating curvaton model [25], which gives a blue-tilted spectrum. On the other hand, small-scale perturbations are determined by a time-dependent radial component of a complex scalar field Φ whose phase direction is the curvaton, which leads to red-tilted spectrum. In the previous model [26], the complex scalar field has a large field value initially and the field value (more precisely the value of the radial direction) decreases during inflation. Since the amplitude of the fluctuations of the curvaton (= the phase direction of Φ) is proportional to $1/|\Phi|$ a blue tilted spectrum is produced. Here we introduce a coupling between

¹ The observational wavelength in the Subaru/HSC ($\sim 600\text{nm}$, r-band) is smaller than the Schwarzschild radius of the lensing objects, PBHs lighter than $\sim 10^{-10}M_{\odot}$.

Φ and the inflaton which stabilize the Φ at $\Phi \simeq 0$ for a large inflaton value. After the inflaton field value becomes some critical value, the stabilization due to the inflaton does not work and Φ rolls down to the true minimum. Thus, contrary to the model in [26], the field value of Φ increases during inflation, which realizes a red-tilted spectrum of the curvaton fluctuations. We considered the PBH production scenarios in two PBH mass cases, (1) DM PBHs with $10^{-13} M_\odot \sim 10^{-11} M_\odot$ and (2) LIGO PBH with $30 M_\odot$, and examine our axion-like curvaton model can explain DM PBHs or LIGO PBHs without conflicting with current observational constraints. In estimating the PBH abundance we take into account the effect of the non-Gaussianity of the curvaton perturbations.

In Sec. II, we explain the axion-like curvaton model with an inflaton-coupling term and derive the formula of the perturbation spectrum analytically. In Sec. III, we review formulas about PBH formation including non-Gaussianity effect. In Sec. IV, we summarize the evaluation of the secondary GWs in our calculation. In Sec. V, we show the results of the numerical calculation for the power spectrum of the density perturbation, the secondary GWs and the mass spectrum of PBHs. Sec. VI is our conclusion.

II. CURVATON MODEL

Here we describe our curvaton model. We introduce a complex scalar field Φ whose phase direction plays a role of the curvaton. The complex scalar Φ has Higgs-like potential, coupling with an inflaton field ϕ and a linear term as

$$V_\Phi = \frac{\lambda}{4}(|\Phi|^2 - v^2)^2 + g\phi^2|\Phi|^2 - v^3\epsilon(\Phi + \Phi^*), \quad (1)$$

where λ and g are coupling constants, v is the vacuum expectation value after inflation, and we assume that the last term is small $\epsilon \ll 1$.

First, let us explain the classical dynamics of Φ in our model. During an early stage of inflation ($\phi \gtrsim (\lambda/g)^{1/2} v$), the $\Phi - \phi$ coupling term fixes Φ near the origin. In a late stage, the inflaton field value ϕ becomes smaller and Φ starts to roll down its Higgs-like potential. When the scalar rolls down from the *exact* origin, quantum fluctuation of Φ given by $H/(2\pi)$ (H : Hubble parameter) affects its classical dynamics and hence the evolution of Φ does not follow the classical equation of motion. In such a case we should use the stochastic formalism for the complex scalar dynamics [29]. To avoid this complexity, we add the small linear term $-v^3\epsilon(\Phi + \Phi^*)$ to the potential. The linear term slightly shifts the stabilized field value of Φ as $\Phi \sim \epsilon v / \lambda$ which is assumed to be a few Hubble away from the origin. Then the scalar Φ rolls down the potential quickly and the classical dynamics dominate the quantum fluctuations. Moreover, the small shift term also avoids the Cosmic string problem.

Suppose that the scalar Φ rolls down the Higgs-like potential at t_{pbh} , in which the subscript "pbh" means the horizon crossing of the perturbation with the PBH scale $k_{\text{pbh}} \simeq 10^5 \text{ Mpc}^{-1}$ (LIGO-PBH) and 10^{12} Mpc^{-1} (DM-PBH) during inflation. The effective mass of Φ is given by

$$m_\varphi^2[|\Phi|, \phi] = \frac{1}{2} \frac{\partial^2}{\partial |\Phi|^2} V_\Phi = \frac{\lambda}{2} (3|\Phi|^2 - v^2) + g\phi^2. \quad (2)$$

Φ starts to roll down when $m_\varphi[|\Phi| = 0, \phi = \phi(t_{\text{pbh}})] \simeq 0$ or

$$g \simeq \frac{\lambda}{2} \left(\frac{v}{\phi(t_{\text{pbh}})} \right)^2. \quad (3)$$

In our calculation, we assume the large effective mass compared to the Hubble parameter during inflation $\lambda v^2 \gg H^2$ to achieve the large tilt of the power spectrum. Since the curvaton is trapped by the steep potential until t_{pbh} , the choice of the initial condition hardly affects the results.

Next, we evaluate the fluctuations of the complex scalar Φ which lead to the curvature perturbations. A peak-like spectrum of the perturbations requires red-tilted shape at $k_{\text{pbh}} < k$ and blue-tilted shape at $k < k_{\text{pbh}}$. We explain the mechanism of generating tilts in the following.

We temporarily write Φ as $\Phi = (\Phi_0 + \varphi)e^{i\theta}$ with the classical solution Φ_0 , and the perturbations φ and θ . We define the canonical field $\tilde{\sigma} = \theta\Phi_0$ as the temporal curvaton. The temporal curvaton becomes the ordinary curvaton σ defined by $\Phi = (v + \varphi)e^{i\sigma/v}$ in the limit $\Phi_0 \rightarrow v$.

During inflation, φ and $\tilde{\sigma} = \theta\Phi_0$ acquire fluctuations with amplitude $H/(2\pi)$ at horizon crossing,

$$\left(\frac{H}{2\pi} \right)^2 = \mathcal{P}_\varphi(k, t_k) = \Phi_0(t_k)^2 \mathcal{P}_\theta(k, t_k) \quad \Rightarrow \quad \mathcal{P}_\theta(k, t_k) = \left(\frac{H(t_k)}{2\pi\Phi_0(t_k)} \right)^2. \quad (4)$$

Since $\Phi_0(t)$ grows exponentially with time (See Fig.1), $\mathcal{P}_{\theta}(k, t_k)$ is sharply red-tilted around t_{pbh} .

The positive mass damps perturbations and makes them blue tilted. The temporal curvaton have the effective mass \tilde{m}_σ through the linear term as

$$\begin{aligned} -v^3 \epsilon (\Phi + \Phi^*) &= -2v^3 \epsilon \Phi_0 \cos\left(\frac{\tilde{\sigma}}{\Phi_0}\right) \simeq -2v^3 \epsilon \Phi_0 + \epsilon v^2 \frac{v}{\Phi_0} \tilde{\sigma}^2 = -2v^3 \epsilon \Phi_0 + \tilde{m}_\sigma \tilde{\sigma}^2, \quad , \\ \tilde{m}_\sigma^2 &= \epsilon v^2 \frac{v}{\Phi_0}. \end{aligned} \quad (5)$$

We choose a small ϵ enough to achieve $\tilde{m}_\sigma^2 > H^2$ at $\Phi_0 \sim H$ and $\tilde{m}_\sigma^2 < H^2$ at $\Phi_0 \sim v$. Using the equation of motion on the perturbation in Eq.(A9), we get the damping factor on $\tilde{\sigma}$ as

$$\ln R_k := \ln\left(\frac{\tilde{\sigma}_k(t_{\text{end}})}{\tilde{\sigma}_k(t_k)}\right) = -\frac{3}{2} \int_{t_k}^{t_{\text{pbh}}} H \text{Re} \left[1 - \sqrt{1 - \left(\frac{2\tilde{m}_\sigma}{3H}\right)^2} \right] dt, \quad (6)$$

in which t_{end} and t_k denote the times at the end of inflation and at the horizon crossing of the perturbation σ_k , respectively. Since \tilde{m}_σ is larger than Hubble before Φ_0 rolls down, the damping factor for $k < k_{\text{pbh}}$ is approximately written as

$$\ln R_k \simeq -\frac{3}{2} \int_{t_k}^{t_{\text{end}}} H dt = -\frac{3}{2} (N(t_{\text{pbh}}) - N(t_k)) \sim \ln\left(\frac{k}{k_{\text{pbh}}}\right)^{3/2} \quad (7)$$

where N is e-foldings defined by $N(t) = \ln(a(t)/a(t_{\text{end}}))$. Thus, for the perturbation with $k < k_{\text{pbh}}$, the power spectrum is blue-tilted $\mathcal{P}_\sigma \propto k^3$.

On the other hand, the radial direction φ mostly has large positive mass $m_\varphi[\varphi, \phi]$ compared to Hubble constant during inflation. Thus, φ is highly suppressed and negligibly small. After inflation, only the angular perturbation is left.

We assume that the curvaton obtains the axion-like potential through some non-perturbative effect as

$$V_\sigma = \Lambda^4 \left[1 - \cos\left(\frac{\sigma}{v}\right) \right] \simeq \frac{1}{2} m_\sigma^2 \sigma^2 = \frac{1}{2} m_\sigma^2 v^2 \theta^2 \quad (8)$$

with $m_\sigma = \Lambda^2/v$. We focus on the density perturbation of the curvaton

$$\frac{\delta \rho_{\sigma;k}}{\rho_\sigma} = 2 \frac{\sigma_k}{v \theta_i} = 2 \frac{\delta \theta_k}{\theta_i} \quad (9)$$

with the misalignment angle θ_i and $\sigma_k \rightarrow v \delta \theta$ after the curvaton rolls down²

Calculating the PBH production, we use the curvature perturbation ζ than the density perturbation $\delta \rho$. The density perturbation contains both contributions from the inflaton and the curvaton. With the energy ratio of the curvaton and the inflaton $r = \rho_\sigma/\rho_I$, the curvature perturbation is given by

$$\begin{aligned} \zeta &= -\frac{H}{\dot{\rho}} \delta \rho = -\frac{H}{\dot{\rho}_I + \dot{\rho}_\sigma} (\delta \rho_I + \delta \rho_\sigma) = \frac{\dot{\rho}_I}{\dot{\rho}_I + \dot{\rho}_\sigma} \left(\frac{-H \delta \rho_I}{\dot{\rho}_I} \right) + \frac{\dot{\rho}_\sigma}{\dot{\rho}_I + \dot{\rho}_\sigma} \left(\frac{-H \delta \rho_\sigma}{\dot{\rho}_\sigma} \right) \\ &= \frac{4}{4+3r} \left(\frac{-H \delta \rho_I}{\dot{\rho}_I} \right) + \frac{3r}{4+3r} \left(\frac{-H \delta \rho_\sigma}{\dot{\rho}_\sigma} \right) \end{aligned} \quad (10)$$

where we use $\dot{\rho}_I = -4H\rho_I$ and $\dot{\rho}_\sigma = -3H\rho_\sigma$.

From Eq.(7)-(10), the curvature perturbation is finally given by

$$\begin{aligned} \mathcal{P}_\zeta(k, t_{\text{end}}) &= \left(\frac{3r}{4+3r} \right)^2 \left(\frac{2}{3\theta_i} \right)^2 \mathcal{P}_\theta(k, t_k) R_k^2 \\ &= \left(\frac{2r}{4+3r} \right)^2 \left(\frac{H(t_k)}{2\pi\Phi(t_k)\theta_i} \right)^2 R_k^2. \end{aligned} \quad (11)$$

We are interested in the curvature perturbation after the curvaton decay into the radiation after inflation. Although r is small during inflation, r grows after inflation since the curvaton behave as matter-like $\rho_\sigma \propto a^{-3}$ until the curvaton decay. In the following, r denotes the ratio at the curvaton decay. We make a list of typical parametrization in Table I and Eq.(32). With $r \sim \mathcal{O}(0.1)$, we take the curvaton decay temperature $T_\sigma \sim 10^7 \text{ GeV}$ (See the detailed discussion in Appendix B).

² The minimum of phase direction of the potential is determined by the linear term for $\Phi_0 \ll v$. This minimum, in general, is different from the minimum of Eq. (8), which results in the misalignment angle θ_i .

III. PBH PRODUCTION

In our model, the PBH production occurs during the radiation-dominated era. We briefly summarize the useful formulas to calculate PBH mass distribution. In the radiation-dominated era, over density regions collapse into black holes. The scale of the perturbation k mainly decides the PBH mass as [24]

$$\begin{aligned}
M(k) &= \gamma \rho_r \frac{4\pi}{3} H^{-3} \Big|_{k=aH}, \\
&\simeq 10^{-12} M_\odot \left(\frac{\gamma}{0.2} \right) \left(\frac{g_*}{106.75} \right)^{-1/6} \left(\frac{k}{1.55 \times 10^{12} \text{ Mpc}^{-1}} \right)^{-2}, \\
&\simeq 10^{-12} M_\odot \left(\frac{\gamma}{0.2} \right) \left(\frac{g_*}{106.75} \right)^{-1/2} \left(\frac{T}{9.75 \times 10^4 \text{ GeV}} \right)^{-2}, \\
&\simeq 30 M_\odot \left(\frac{\gamma}{0.2} \right) \left(\frac{g_*}{10.75} \right)^{-1/6} \left(\frac{k}{3.43 \times 10^5 \text{ Mpc}^{-1}} \right)^{-2}, \\
&\simeq 30 M_\odot \left(\frac{\gamma}{0.2} \right) \left(\frac{g_*}{10.75} \right)^{-1/2} \left(\frac{T}{31.6 \text{ MeV}} \right)^{-2}, \tag{12}
\end{aligned}$$

where ρ_r is the radiation energy density and γ is the ratio of PBH mass to the horizon mass. We use the simple analytical estimation $\gamma = 3^{-3/2} \simeq 0.2$ [18] in this paper.

The power spectrum of the curvature perturbations \mathcal{P}_ζ determines the PBH production rate. At first, we assume the curvature spectrum can be well approximated to follow the Gaussian distribution. We take non-Gaussianity into account later. PBH production depends on the coarse-grained density perturbation over the Horizon. The density perturbation in comoving gauge is related to the curvature perturbation as $\delta = (4/9)(k/aH)\zeta$. Once the coarse-grained density perturbation exceeds the threshold value δ_c , the horizon mass collapses into black holes. In this paper, we take the threshold as $\delta_c = 0.4$ [30]. The coarse-grained density perturbation is given by

$$\begin{aligned}
\delta_W(x; R) &:= \int d^3y W(|x-y|; R) \delta(y) \\
&= \int \frac{d^3k}{(2\pi)^3} \tilde{W}(k; R) e^{ik \cdot x} \delta_k \tag{13}
\end{aligned}$$

and its correlation function is

$$\langle \delta_W^2 \rangle_{(M(k))} = \langle \delta_W(x; k^{-1}) \delta_W(x; k^{-1}) \rangle = \int d\ln q \tilde{W}^2(q; k^{-1}) \frac{16}{81} (q/k)^4 \mathcal{P}_\zeta(q) T(q, k^{-1})^2 \tag{14}$$

where $\tilde{W}(k; R)$ is a window function in momentum space and $T(k, \eta)$ the transfer function. Since we assume that the curvaton has already decayed into the radiation before the PBH production, we use the transfer function in the radiation-dominated era,

$$T(k, \eta) = 3 \frac{\sin(k\eta/\sqrt{3}) - k\eta/\sqrt{3} \cos(k\eta/\sqrt{3})}{(k\eta/\sqrt{3})^3}. \tag{15}$$

Note that the choice of the window function causes $\mathcal{O}(1)$ uncertainties on $\langle \delta_W^2 \rangle$ [31]. We calculate $\langle \delta_W^2 \rangle$ using Gaussian type $\tilde{W}(k, R) = e^{-(kR)^2/2}$, real-space top-hat type $\tilde{W}(k, R) = 3(\sin(kR) - kR \cos(kR))/(kR)^3$ and delta-function type $\tilde{W}(k, R)^2 = \delta(kR - 1)$. For the scale invariant case $\mathcal{P}_\zeta(k) = A_s$, $\langle \delta_W^2 \rangle$ depends on the choice of the window function as [31]

$$\langle \delta_W^2 \rangle = \begin{cases} 1.06 A_s & (\text{real-space top-hat}) \\ 0.191 A_s & (\text{delta-function}) \\ 0.0867 A_s & (\text{Gaussian}). \end{cases} \tag{16}$$

Once $\langle \delta_W^2 \rangle$ is given, one can estimate the PBH production rate as

$$\beta_{(M)} = \int_{\delta_c}^{\infty} \frac{d\delta}{\sqrt{2\pi \langle \delta_W^2 \rangle_{(M)}}} e^{-\frac{\delta^2}{2\langle \delta_W^2 \rangle_{(M)}}} \sim \frac{1}{\sqrt{2\pi}} \frac{\sqrt{\langle \delta_W^2 \rangle}}{\delta_c} e^{-\frac{\delta_c^2}{2\langle \delta_W^2 \rangle_{(M)}}}. \tag{17}$$

The mass spectrum of PBH is [24]

$$\begin{aligned}
f(M) &= \frac{d\Omega_{\text{PBH}}}{d\ln M} \frac{1}{\Omega_{\text{DM}}} = \frac{\gamma \rho_r(t_M) \beta(M)}{\rho_m(t_M)} \frac{\Omega_m}{\Omega_{\text{DM}}} \\
&\simeq \left(\frac{\beta(M)}{1.0 \times 10^{-14}} \right) \left(\frac{\gamma}{0.2} \right)^{3/2} \left(\frac{106.75}{g_*(T_M)} \right)^{1/4} \left(\frac{0.12}{\Omega_{\text{DM}} h^2} \right) \left(\frac{M}{10^{-13} M_\odot} \right)^{-1/2} \\
&\simeq \left(\frac{\beta(M)}{1.8 \times 10^{-8}} \right) \left(\frac{\gamma}{0.2} \right)^{3/2} \left(\frac{10.75}{g_*(T_M)} \right)^{1/4} \left(\frac{0.12}{\Omega_{\text{DM}} h^2} \right) \left(\frac{M}{M_\odot} \right)^{-1/2}.
\end{aligned} \tag{18}$$

Here the subscription "m" denotes the matter (baryon+DM). With use of $f(M)$, the total fraction of PBH in DM is rewritten as

$$\frac{\Omega_{\text{PBH}}}{\Omega_{\text{DM}}} = \int d\ln M f(M). \tag{19}$$

It is known that $\Omega_{\text{PBH}}/\Omega_{\text{DM}} \simeq 10^{-3}$ [13] explains the binary black hole merger event rate observed by the LIGO. Note that the above-mentioned PBH production mechanism has some uncertainties on γ , δ_c and the choice of window functions. In this paper, we chose the conservative values for γ and δ_c .

So far we have assumed that the curvature perturbations are Gaussian. Now we take into account the effect of non-Gaussianity. In fact, it is known that the curvaton produces non-Gaussianity in curvature perturbations. Here we briefly summarize our treatment of the non-Gaussianity in this paper based on [32, 33].

Non-Gaussian distribution with the local type bispectrum can be written as

$$\zeta(x) = \zeta_g(x) + \frac{3}{5} f_{\text{NL}} \left(\zeta_g^2(x) - \langle \zeta_g^2(x) \rangle \right) \tag{20}$$

where $\zeta_g(x)$ follows a Gaussian distribution. In curvaton models, the non-Gaussianity parameter f_{NL} is determined by the ratio r of the curvaton density to radiation density at the curvaton decay and is written as

$$f_{\text{NL}} = \frac{5}{12} \left(-3 + \frac{4}{r} + \frac{8}{4+3r} \right). \tag{21}$$

There is one difficulty in considering the non-Gaussian effect. The f_{NL} is defined in the curvature perturbation ζ while the PBH formation is calculated by the coarse-grained comoving density perturbation. Here we recalculate $\beta(M)$ using ζ at the horizon crossing and estimate the non-Gaussian effect.

Non-Gaussianity modifies our discussion in the two points. First, non-Gaussianity could increase the PBH fraction $\beta(M)$ to amplify the probability at $\delta \simeq \delta_c$ of the distribution function. Using Eq.(20). The PBH fraction including non-Gaussianity $\beta(\langle \zeta_g^2 \rangle, f_{\text{NL}})$ is esitimated as [33]

$$\beta(\langle \zeta_g^2 \rangle, f_{\text{NL}}) \simeq \frac{1}{\sqrt{2\pi}} \left(\frac{1}{y_{c+}} e^{-\frac{y_{c+}^2}{2}} + \frac{1}{y_{c-}} e^{-\frac{y_{c-}^2}{2}} \right) \tag{22}$$

where the $y_{c\pm}$ is given by

$$y_{c\pm} = \frac{1}{\sqrt{\langle \zeta_g^2 \rangle}} \frac{5}{6f_{\text{NL}}} \left[-1 \pm \sqrt{1 + \frac{12}{5} f_{\text{NL}} \left(\frac{3}{5} f_{\text{NL}} \langle \zeta_g^2 \rangle + \zeta_c \right)} \right], \tag{23}$$

where the critical curvature ζ_c depends on the critical density $\delta_c = 0.4$ and the choice of window function. We approximately use the Eq.(16) as the relation between ζ_c and δ_c :

$$\zeta_c = \begin{cases} 0.389 & \text{(real-space top-hat)} \\ 0.915 & \text{(delta-function)} \\ 1.36 & \text{(Gaussian).} \end{cases} \tag{24}$$

Since the curvature perturbation with k at the peak of the power spectrum dominantly contributes to the PBH production, we approximate $\langle \zeta_g^2 \rangle$ as the peak value $\mathcal{P}_{\zeta_g}(k_{\text{pbh}})$. For a given PBH fraction β_c , f_{NL} effectively lowers the required curvature perturbation $\mathcal{P}_{\zeta_g}(k_{\text{pbh}}) \rightarrow B(f_{\text{NL}}) \mathcal{P}_{\zeta_g}$ given by

$$\beta_c = \beta(\mathcal{P}_{\zeta_g}, f_{\text{NL}} = 0) = \beta(B(f_{\text{NL}}) \mathcal{P}_{\zeta_g}, f_{\text{NL}}). \tag{25}$$

The second effect of non-Gaussianity is that the power spectrum obtains an additional contribution from the second term in Eq. (20), which is written as

$$\mathcal{P}_\zeta(k) = \mathcal{P}_{\zeta_g}(k) + \left(\frac{3}{5}f_{NL}\right)^2 \frac{k^3}{2\pi} \int d^3q \frac{1}{q^3} \frac{1}{|k-q|^3} \mathcal{P}_{\zeta_g}(q) \mathcal{P}_{\zeta_g}(|k-q|). \quad (26)$$

We define the amplification factor of the power spectrum at the peak value as

$$\sqrt{Q(\mathcal{P}_{\zeta_g}(k_{\text{pbh}}), f_{NL})} = \frac{\mathcal{P}_\zeta(k_{\text{pbh}})}{\mathcal{P}_{\zeta_g}(k_{\text{pbh}})}. \quad (27)$$

In the following calculation, we include the effect of non-Gaussianity on both the PBH production and perturbations.

IV. CONSTRAINTS OF THE SECONDARY GRAVITATIONAL WAVE

The large curvature perturbations produce the secondary gravitational waves [28, 34, 35]. We calculate the differential density parameter of the produced GWs. The GWs are mainly produced when the peak value of the curvature re-enters the horizon in the radiation-dominated era. After production the GW energy density decreases by the cosmic expansion, and at present the density parameter of the produced GWs is [31]:

$$\Omega_{GW}(k, t_0) = \left(\frac{a_c^2 H_c}{a_0^2 H_0} \right)^2 \Omega_{GW}(\eta_c, k) \simeq 0.83 \left(\frac{g_c}{10.75} \right)^{-1/3} \Omega_{r,0} \Omega_{GW}(\eta_c, k), \quad (28)$$

where η_c is some time when the secondary GW generation effectively finishes. For $\eta > \eta_c$, the GWs behave as radiation $\rho_{GW} \propto a^{-4}$. Here g_c is the degrees of freedom of the radiation at η_c . In our case, we assume $g_c = 10.75$ for LIGO-PBH case and $g_c = 106.75$ for DM-PBH case.

$\Omega_{GW}(\eta_c, k)$ is calculated using the power spectrum of the curvature perturbations $\mathcal{P}_\zeta(kx)$ as [24]

$$\Omega_{GW}(\eta_c, k) = \left\langle \frac{8}{243} \int_0^\infty dy \int_{|1-y|}^{1+y} dx \frac{y^2}{x^2} \left(1 - \frac{(1+y^2-x^2)^2}{4y^2}\right)^2 \mathcal{P}_\zeta(kx) \mathcal{P}_\zeta(ky) \left[\frac{k^2}{a(\eta)} \int_\eta^\eta d\bar{\eta} a(\bar{\eta}) g_k(\eta; \bar{\eta}) f(ky, kx, \bar{\eta}) \right]^2 \right\rangle, \quad (29)$$

where $\langle \dots \rangle$ means the time average over η_c , $T(\eta, k)$ is the transfer function of the radiation, g_k is the Green function

$$T(\eta, k) = 9\sqrt{3} \frac{\sin(k\eta/\sqrt{3}) - (k\eta/\sqrt{3})\cos(k\eta/\sqrt{3})}{(k\eta)^3},$$

$$g_k(\eta, \bar{\eta}) = \frac{\sin(k(\eta - \bar{\eta}))}{k} \theta(\eta - \bar{\eta}). \quad (30)$$

$f(k_1, k_2, \eta)$ is given by

$$f(k_1, k_2, \eta) = \left[2T(k_1, \eta)T(k_2, \eta) + \left(\frac{\dot{T}(k_1, \eta)}{H(\eta)} + T(k_1, \eta) \right) \left(\frac{\dot{T}(k_2, \eta)}{H(\eta)} + T(k_2, \eta) \right) \right]. \quad (31)$$

Considering the non-Gaussianity, we multiply the factor $B(f_{NL})^2 Q(B(f_{NL})\mathcal{P}_{\zeta_g}(k_{\text{pbh}}), f_{NL})$ [see, Eq.(25) and Eq.(27)] to the Ω_{GW} .

V. RESULTS

A. Classical dynamics of the complex scalar

During inflation, Φ_0 obeys the equation of motion Eq.(A5). We numerically solve the equation and obtain the classical dynamics for parameters which are appropriate for PBH-DM and LIGO-PBH. For simplicity, we use the chaotic Inflation as background inflaton dynamics. We assume the inflaton potential as $V_{\text{inf}} = m_\phi^2 \phi^2/2$ with $m_\phi = (5 \times 10^{-6} M_{pl}) \simeq 10^{13} \text{ GeV}$ (M_{pl} : reduced Planck mass). We take the initial inflaton value $\phi_{in} = 15.6 M_{pl}$ which achieves the e-foldings $N > 55$.

We take the typical parameter for PBH-DM and LIGO-PBH as

$$\nu_{DM} = 3.42 \times 10^{-2} M_{pl}, \quad \lambda_{DM} = 5 \times 10^{-5}, \quad \epsilon_{DM} = 7.96 \times 10^{-10}, \quad g_{DM} = 4.2 \times 10^{-10}$$

$$\nu_{LIGO} \simeq 5.73 \times 10^{-2} M_{pl}, \quad \lambda_{LIGO} = 5 \times 10^{-5}, \quad \epsilon_{LIGO} = 3.06 \times 10^{-10}, \quad g_{LIGO} = 7.08 \times 10^{-10} \quad (32)$$

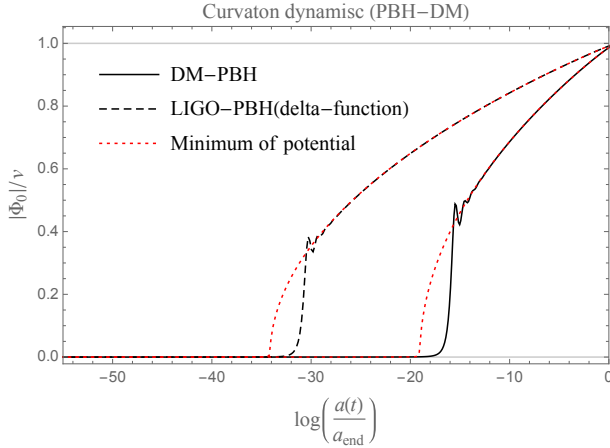


FIG. 1. The field value of $|\Phi_0|$ for each time during inflation for DM-PBH case (black solid line) and LIGO-DM case (black dashed line). The field value is normalized with v . The horizontal axis expresses the scale factor normalized with the inflation end $N(t) = \log(a(t)/a_{end})$. Red lines express the potential minimum for DM-PBH and LIGO-DM cases.

and we slightly change the parameter v_{LIGO} for each window selection on LIGO-PBH since the different window function produces PBHs with different masses.

We show the results in Fig. 1. In the early stage of inflation, Φ_0 is fixed near the origin due to the inflaton-coupling $g\phi^2|\Phi|^2$. After the perturbation with the PBH scale crosses the horizon, the effective mass near the origin becomes tachyonic and Φ_0 rolls down the Higgs-like potential. Since we introduce $U(1)$ symmetry breaking linear term $-\nu^3\epsilon(\Phi+\Phi^*)$, the complex scalar field rolls down to $\arg(\Phi)=0$ direction. The red lines in Fig. 1 show the minimum of the potential. At t_{pbh} , the potential minimum shifts toward v . At that moment, Φ_0 is left near the origin. Due to the small linear term, Φ_0 has nonzero value and grows exponentially to follow the potential. When Φ_0 catches up with the potential minimum, Φ_0 oscillates around the minimum. In Fig. 1, you can see the oscillating field dynamics (black lines) around the potential minimum (red lines). Finally, the inflation-coupling vanishes and the potential minimum becomes v .

We also check the consistency of the calculation. In the previous calculation, we assumed that the quantum perturbation do not disturb the classical dynamics, which means that

$$\frac{|\Phi|}{H/(2\pi)} > 1 \quad , \quad \frac{|\dot{\Phi}|}{H^2/(2\pi)^2} > 1 \quad (33)$$

when Φ_0 starts to roll down. We numerically confirm that $2\pi|\Phi|/H > 3$ and $(2\pi)^2|\dot{\Phi}|/H^2 > 15$ at the time $m_\varphi^2 = 0$.

In our numerical calculation, we include the energy density of the complex scalar Eq. (1) into the total energy density of the universe during inflation. During inflation, the complex scalar slightly affects the inflation dynamics. The energy ratio of the complex scalar to the inflaton has the maximum value (17%) at t_{pbh} but decreases quickly as the complex scalar rolls down the Higgs-like potential.

B. The perturbation of the curvaton

To explain how our model produces the sharp peak in the power spectrum, we plot the angular perturbation $\delta\theta_k$ at each horizon-crossing time t_k and t_{end} in Fig. 2 where $\delta\theta_k(t_{end})$ is

$$\delta\theta_k(t_{end}) = \delta\theta_k(t_k)R_k = \left(\frac{H(t_k)}{2\pi\Phi(t_k)} \right) R_k \propto \sqrt{\mathcal{P}_\zeta(k, t_{end})} \quad (34)$$

for the LIGO-PBH case with delta-function window.

The shape of $\delta\theta_k(t_k)$ (solid line in Fig. 2) mainly follows $\propto |\Phi_0|^{-1}$ in Fig. 1. Using the damping factor $R_k \simeq (k/k_{pbh})^{\frac{3}{2}}$ in Eq. (7), we get the damped angular perturbation (dotted line in Fig. 2). Since the damping effect mainly works until $t < t_{pbh}$, the small-scale perturbations with $k > k_{pbh}$ do not suffer from the damping effect.

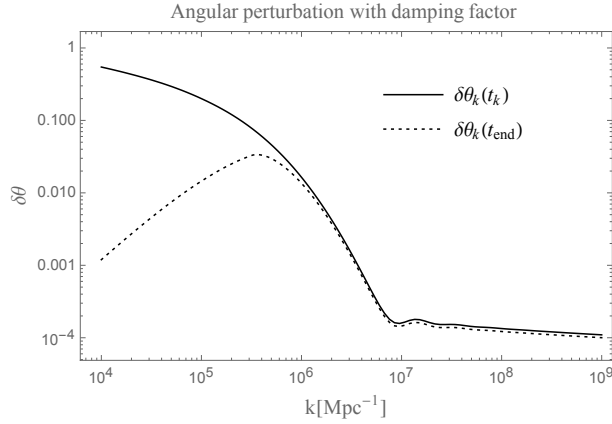


FIG. 2. The angular perturbation $\delta\theta_k$ on the LIGO-PBH(delta-function window) case. The solid line expresses the angular perturbation at t_k . Due to the positive effective mass, the large-scale perturbation with $k < k_{\text{pbh}}$ is damped (dotted line).

TABLE I. Table for the typical value of r and θ_i

(r, θ_i)	LIGO-PBH	DM-PBH
Gaussian window	(1.0, 0.0587)	(1, 0.0537)
delta-function window	(0.5, 0.0741)	(0.5, 0.0680)
Top-hat window	(0.5, 0.127)	(0.5, 0.115)

We list the required values to produce enough amount of PBHs for each curvaton parameter in Eq.(32). We try the three window functions and with non-Gaussianity. Note that the parameter of the Gaussian window case is constrained by $\delta\rho_\sigma/\rho_\sigma < 1$ discussed in Chapter V E.

C. Curvature power spectrum and PBH production

In order to calculate the PBH mass spectrum, we should fix two more parameters, the curvaton energy ratio r and the misalignment angle θ_i , which affect the curvature spectrum as $\mathcal{P}_\zeta \propto (2r/(4+3r))^2 \theta_i^{-2}$. We determine r and θ_i in the following way. For the given PBH density $\Omega_{\text{PBH}}/\Omega_{\text{DM}} = 1$ (DM-PBH) or $\Omega_{\text{PBH}}/\Omega_{\text{DM}} = 10^{-3}$ (LIGO-PBH), we search the allowed parameter region of r and θ_i to achieve the required $\Omega_{\text{PBH}}/\Omega_{\text{DM}}$. We list the typical values of r and θ_i for each window function in Table(I). The different window functions require the different values of \mathcal{P}_ζ to produce enough amount of PBHs. As is seen from Eq.(16), the Gaussian window function requires the largest \mathcal{P}_ζ to produce a sufficient number of PBHs and the top-hat window function requires the smallest.

For fixed $\Phi_0(t)$, r and θ_i , we calculate the power spectrum of the curvature perturbations $\mathcal{P}_\zeta(k)$ [Eq.(11)] which is shown in Fig.3. We plot $\mathcal{P}_\zeta(k)$ for the three window function cases: Gaussian window case (red lines), delta-function window case (black lines) and top-hat window case (blue lines). We compare the results with/without non-Gaussianity effect (solid lines/dotted lines). Since we fix the PBH fraction, the non-Gaussianity effectively lowers the required \mathcal{P}_ζ as explained in Eq.(25).

The powerspectrum of the curvature perturbations is constrained by CMB μ -distortion [36, 37] and big bang nucleosynthesis(BBN) [38]. The curvature perturbations on small scales dissipate through the Silk damping into the radiation. Such energy transfer distorts the spectrum of the CMB (μ -distortion). When the large curvature perturbations re-enter the horizon during BBN, they modifies the freeze-out value of the neutron-proton ratio. This modification is constrained by the observed ${}^4\text{He}$ abundance [39]. In Fig.3, we confirm that our model avoids those constraints on $\mathcal{P}_\zeta(k)$. This is because our model produces the steep spectrum of $\mathcal{P}_\zeta(k)$ on the small scales by the positive effective mass as can be seen in Eq.(7).

Next we discuss the the PBH mass spectrum $f(M)$. The PBH mass spectra in our model are shown in Fig.4 for the three window function cases: delta-function window case (black lines) and top-hat window function case (blue lines). Since we fix the PBH mass density, the mass spectrum depends only on the choice of the window function, which mainly changes the peak width of each distribution.

PBH distribution is severely constrained by mainly two types of observation.

- For PBHs with $10^{-10} - 10 M_\odot$, microlensing experiments put the severe constraints. Massive compact object works as a gravitational lens and amplifies the brightness of the background stars on the line of sight. Microlensing experiments observe the transient amplification of the brightness in some time domain. Subaru/HSC surveyed the An-

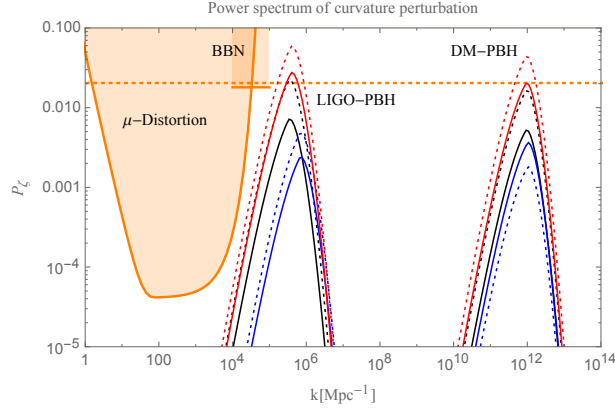


FIG. 3. \mathcal{P}_ζ for each momentum k normalized with Mpc^{-1} for DM-PBH (peak around $k = 10^6 \text{ Mpc}^{-1}$) and LIGO-DM (peak around $k = 10^{12} \text{ Mpc}^{-1}$). We plot the delta-function window case (black lines), top-hat window function case (blue lines) and Gaussian window function case (red lines). Solid line and dotted line express the case with/without non-Gaussianity. The large curvature perturbation causes the distortion on Planck distribution of the CMB spectrum (μ -Distortion[37]), which is constrained by the COBE/FIRAS [36]. Big bang nucleosynthesis (BBN) also constrain the large curvature perturbation [38]. The constraint from the isocurvature (orange dotted horizontal line) in Eq.(36) denies the Gaussian window function case.

dromeda galaxy (M31) [22] and MACHO/EROS/OGLE surveyed the Large and Small Magellanic Cloud [19–21] and put the constraints on the abundance of the massive compact objects. They have excluded the DM-PBH scenario with monochromatic mass $(10^{-10} - 10) M_\odot$. As for smaller mass than $10^{-10} M_\odot$ the constraint becomes much weaker since the observational wavelength is comparable to the Schwarzschild radius of the lensing objects [24, 40–42]. We express the region with wave-effect as a dotted line in Fig.4.

- For large mass $\text{PBH} > 10^2 M_\odot$, constraints are given by the mass accretion process onto PBHs. In the early universe, the gas accretion injects energy into CMB. The previous study [43] considered two energy injection calculation (collisional ionization/photoionization). Freely-floating black holes in the interstellar medium are constrained by the X-ray emission from its accretion gas [44].
- Other constraints: for PBHs with smaller mass than $10^{-13} M_\odot$, a white dwarf constrains its abundance(WD). When a PBH collides with a white dwarf, localized heating on its trajectory causes the explosion [45].

Although the PBH mass spectrum $f(M)$ is already severely constrained, our model avoids these constraints by the sharp peak spectrum.

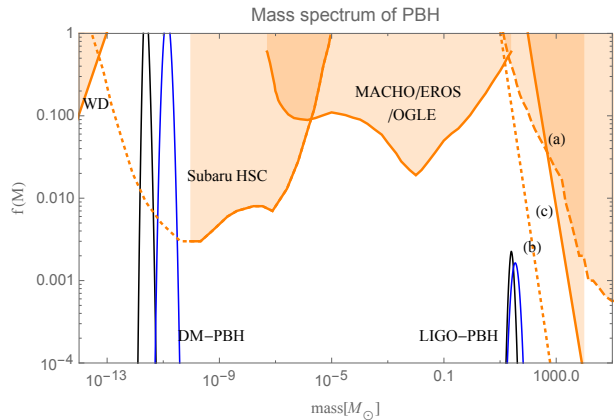


FIG. 4. PBH mass spectra $f(M)$ of DM-PBH around $10^{-12} M_\odot$ and LIGO-DM around $30 M_\odot$ for the two window function choices: delta-function window (black lines) and top-hat window function (blue lines). The region labeled "WD" show the constraint from PBH collisions with a white dwarf [45]. The regions labeled "Subaru/HSC" [22] and "MACHO/EROS/OGLE" [19–21] are constraints from microlensing experiments (the dotted line in shows the the constraint without "wave effect"[24, 40–42]). "(a)" and "(b)" are the constraints from the accretion effect on CMB [43] with two energy injection calculation (collisional ionization/photo-ionization). "(c)" is the constraint by the X-ray emission from accretion gas around PBH [44].

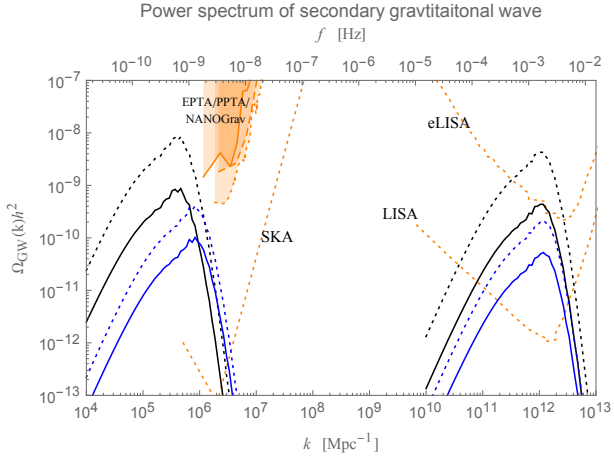


FIG. 5. The differential energy density of secondary gravitational waves for each momentum k . The power spectra of LIGO-PBH (peak around 10^5 Mpc^{-1}) and DM-PBH (peak around 10^{12} Mpc^{-1}) are plotted for the different window functions (black: delta-function window, blue: Top-hat window). The solid and dotted lines are the power spectra with/without non-Gaussianity. The Pulsar Timing Array experiments constrain the energy density around 10^6 Mpc^{-1} , and the future space-borne GW interferometer (eLISA/LISA) would constraints around 10^{12} Mpc^{-1} . The current PTA constraints comes from EPTA [46] (solid line), NANOGrav [47] (Dashed line) and PPTA [48] (dotted line). The future constraints by the eLISA/LISA and SKA [50] are shown by the red dotted lines.

D. Secondary gravitational wave

We numerically calculate the secondary gravitational waves Eq.(28) in Fig.5. In estimating Ω_{GW} we assume that the curvaton has already decayed when the peak of the density perturbation re-enter the horizon. For the typical parameters, the curvaton decays at $T_\sigma = 10^7 \text{ GeV}$ and DM-PBH is produced at 10^5 GeV and LIGO-PBH at 50 MeV .³

Pulsar Timing Array (PTA) experiments put severe constraints on stochastic GWs [46–48] around 10^6 Mpc^{-1} which is also shown in Fig.5. Our model for LIGO-PBH case avoids the current PTA constraints by the sharp peak spectrum. In the future experiments can detect the GWs predicted by the curvaton model. For an example the Square Kilometer Array (SKA) would improve the sensitivity of stochastic GWs around 10^6 Mpc^{-1} [49, 50]. For the stochastic GWs around 10^{12} Mpc^{-1} , eLISA/LISA would put the constraints for DM-PBH scenario [50].

E. Constraint of isocurvature

Although the smaller θ_i enhances $\mathcal{P}_\zeta \propto \theta_i^{-2}$, θ_i is constrained from below by the condition that the energy perturbation should not be larger the mean value, i.e., $\delta\rho_\sigma/\rho_\sigma < 1$. From Eq.(9) the condition can be rewritten as

$$1 > \left(\frac{\delta\rho_\sigma}{\rho_\sigma} \right)^2 = \left(\frac{4+3r}{r} \right)^2 \mathcal{P}_\zeta(k). \quad (35)$$

In this paper, we assume that the PBH production during the radiation-dominated era and $r < 1$, which leads

$$\mathcal{P}_\zeta(k) < \frac{1}{7^2} \simeq 0.0204. \quad (36)$$

The condition Eq.(35) do not hold in Gaussian window function case, which requires the large P_ζ to produce the enough amount of PBHs. In Fig.3, we can see that delta-function window case and top-hat window function case avoids the constraint Eq.(35) with/without non-Gaussianity.

VI. CONCLUSION

In this paper, we have studied the PBH formation model with axion-like particle [26]. We have modified the original model by introducing a coupling with an inflaton field, which leads to a sharp peak in the power spectrum of the curva-

³ The curvature perturbations due to the curvaton before the decay requires the different treatment for calculating the Ω_{GW} . Including the contribution before the curvaton decay, Ω_{GW} of the DM-PBH could slightly change the spectrum shape but the typical value of Ω_{GW} would not change.

ture perturbations. The coupling with inflaton also enable us to choose the mass scale of produced PBHs without tuning of initial field value or the curvaton decay rate. We have also evaluated the non-Gaussianity effect of the curvaton and uncertainty from the choice of the window function. It has been found that our model produces enough amount of PBHs as LIGO events ($30M_{\odot}$) and DM ($10^{-12}M_{\odot}$).

Finally, our calculation has shown that our model is consistent with the current constraints on the curvature perturbation $\mathcal{P}_{\zeta}(k)$ [see, Fig.3], on the PBH mass function $f(M)$ [see, Fig.4] and on the secondary GW Ω_{GW} [see, Fig.5]. Next-generation observations would verify our model through $\mathcal{P}_{\zeta}(k)$ by PTA using SKA and Ω_{GW} or by space gravitational wave interferometers (LISA, eLISA).

ACKNOWLEDGEMENTS

This work was supported by JSPS KAKENHI Grant Nos. 17H01131 (M.K.) and 17K05434 (M.K.), MEXT KAKENHI Grant No. 15H05889 (M.K.), World Premier International Research Center Initiative (WPI Initiative), MEXT, Japan (K.A., M.K., H.N.), JSPS Research Fellowships for Young Scientists (K.A.), and Advanced Leading Graduate Course for Photon Science (K.A., H.N.).

Appendix A: Equation of motion of the curvaton

During inflation, our model assumes the following potential:

$$V_{\Phi} = \frac{\lambda}{4} (|\Phi|^2 - v^2)^2 + g \phi^2 |\Phi|^2 - v^3 \epsilon (\Phi + \Phi^*). \quad (\text{A1})$$

We decompose the complex scalar Φ into a homogeneous classical solution Φ_0 and the perturbation Φ_1 . The action on the FLRW space-time is

$$\begin{aligned} S &= \int d^4x \sqrt{-g} \left(-\frac{1}{2} (\Phi_0 + \Phi_1)_{,\mu} (\Phi_0 + \Phi_1)^*_{,\nu} g^{\mu\nu} - V_{\Phi} [\Phi_0 + \Phi_1] \right) \\ &= \int d\eta d^3x a^4 \left(\frac{1}{2a^2} (|\Phi_0 + \Phi_1|^2 - |\nabla \Phi_1|^2) - V_{\Phi} [\Phi_0 + \Phi_1] \right) \end{aligned} \quad (\text{A2})$$

with $\sqrt{-g} \sim a^3$ and $\Phi' = \partial \Phi / \partial \eta = a \partial \Phi / \partial t = a \dot{\Phi}$. The equation of motion is

$$\begin{aligned} 0 &= \frac{\partial}{\partial \eta} \frac{\delta S}{\delta \Phi'^*} + \frac{\partial}{\partial x^i} \frac{\delta S}{\delta \Phi^*_{,i}} - \frac{\delta S}{\delta \Phi^*} \\ &= \frac{\partial a^2 (\Phi_0 + \Phi_1)'}{\partial \eta} + \frac{\partial a^2 \Phi_{1,i}}{\partial x^i} + a^4 \frac{\partial V_{\Phi} [\Phi_0 + \Phi_1]}{\partial \Phi^*} \\ &= a^2 \left[(\Phi_0 + \Phi_1)'' + 2aH(\Phi_0 + \Phi_1)' + \nabla^2 \Phi_1 + a^2 \frac{\partial V_{\Phi} [\Phi_0 + \Phi_1]}{\partial \Phi^*} \right], \end{aligned} \quad (\text{A3})$$

where

$$\frac{\partial V_{\Phi}}{\partial \Phi^*} = \left(g \phi^2 - \frac{\lambda}{2} (v^2 - |\Phi|^2) \right) \Phi - \epsilon v^3. \quad (\text{A4})$$

The classical solution satisfies Eq.(A3) for $\Phi_1 = 0$:

$$0 = \Phi_0'' + 2aH\Phi_0' + a^2 \left[\left(g \phi^2 - \frac{\lambda}{2} (v^2 - |\Phi_0|^2) \right) \Phi_0 - \epsilon v^3 \right]. \quad (\text{A5})$$

Note that Φ_0 rolls down the Higgs-like potential into $\arg(\Phi_0) = 0$ direction with $\epsilon > 0$.

Inserting the classical motion Eq.(A5) into Eq.(A3), the perturbation Φ_1 satisfies

$$\begin{aligned} 0 &= \Phi_1'' + 2aH\Phi_1' + \nabla^2 \Phi_1 + a^2 \left(\frac{\partial V_{\Phi} [\Phi_0 + \Phi_1]}{\partial \Phi^*} - \frac{\partial V_{\Phi} [\Phi_0]}{\partial \Phi^*} \right) \\ &= a^2 [\ddot{\Phi}_1 + 3H\dot{\Phi}_1 + a^{-2} \nabla^2 \Phi_1 + (u\Phi_1^* + v\Phi_1 + w[\Phi_0, \Phi_1])] \\ u &= \frac{\lambda}{2} \Phi_0^2 \quad , \quad v = g \phi^2 - \frac{\lambda v^2}{2} + \lambda |\Phi_0|^2 \quad , \quad w = \frac{\lambda}{2} (\Phi_1 |\Phi_1|^2 + 2\Phi_0 |\Phi_1|^2 + \Phi_0^* \Phi_1^2). \end{aligned} \quad (\text{A6})$$

We consider the terms up to the second order of the perturbation. With the Fourier-transformation and the diagonalization, the equation of motion is given by

$$\begin{aligned} \left[\partial_t^2 + 3H\partial_t + a^{-2}k^2 + \begin{pmatrix} v & u \\ u^* & v \end{pmatrix} \right] \begin{pmatrix} \Phi_{1;k} \\ \Phi_{1;k}^* \end{pmatrix} &= 0, \\ \left[\partial_t^2 + 3H\partial_t + a^{-2}k^2 + \begin{pmatrix} v+u \\ v-u \end{pmatrix} \right] \frac{1}{\sqrt{2}} \begin{pmatrix} \Phi_{1;k} + \Phi_{1;k}^* \\ -\Phi_{1;k} + \Phi_{1;k}^* \end{pmatrix} &= 0. \end{aligned}$$

where we use that u is real in our calculation.

Comparing $\Phi = (\Phi_0 + \varphi)e^{i\sigma/\Phi_0}$, we get effective masses:

$$\begin{aligned} m_\varphi^2 &= v + u = g\phi^2 - \frac{\lambda v^2}{2} + \frac{3}{2}\lambda|\Phi_0|^2 \quad , \\ \tilde{m}_\sigma^2 &= v - u = g\phi^2 - \frac{\lambda v^2}{2} + \frac{1}{2}\lambda|\Phi_0|^2. \end{aligned} \quad (\text{A7})$$

\tilde{m}_σ^2 reproduces Eq.(5) with $\partial V_0/\partial\Phi^* = 0$.

Assuming that the perturbation is super-horizon $aH \gg k$, Hubble parameter is constant and the solution can be written as $\Phi_{1;k} \pm \hat{\Phi}_{1;k}^* \propto e^{i\omega_k t}$, we approximately solve Eq.(A7) as

$$\begin{aligned} \left[\partial_t^2 + 3H\partial_t + a^{-2}k^2 + m_{\text{eff}}^2 \right] e^{i\omega_k t} &= 0, \\ \omega_k &= \frac{3}{2}iH \left(1 \pm \sqrt{1 - \left(\frac{2m_{\text{eff}}}{3H} \right)^2} \right). \end{aligned} \quad (\text{A8})$$

In $m_{\text{eff}} > 0$, the perturbations are strongly damped as

$$\frac{\partial \ln |\Phi_{1;k}|}{\partial t} = -\frac{3}{2}H \text{Re} \left[1 - \sqrt{1 - \left(\frac{2m_{\text{eff}}}{3H} \right)^2} \right]. \quad (\text{A9})$$

Appendix B: The curvaton energy ratio

In this section, we summarize the curvaton dynamics in the radiation-dominated era [27]. We evaluate the energy ratio $r = \rho_\sigma/\rho_I$ when both curvaton and inflaton decay into the radiation.

To calculate the curvaton energy ratio, we define some notations: t_{end} when the inflaton ends, t_R when the inflaton decays, $t_{\sigma;\text{Osl}}(H = m_\sigma)$ when the curvaton starts to oscillates and $t_{\sigma;\text{dec}}$ when the curvaton decays. We focus on the case $t_{\text{end}} < t_{\sigma;\text{Osl}} < t_R < t_{\sigma;\text{dec}}$ to achieve the large r value. We can rewrite the condition as $m_\phi > m_\sigma > \Gamma_R > \Gamma_\sigma$ with the decay rate into the radiation of inflaton Γ_R and that of the curvaton Γ_σ .

The energy ratio is given by $r = (T_R/T_\sigma)v^2\theta_i^2/(6M_{pl}^2)$ [27]. We use the instant reheating assumption:

$$\Gamma_R = \sqrt{\frac{\pi^2}{30}(g_* T_R^4/3M_{pl}^2)} \quad , \quad \Gamma_\sigma = \sqrt{\frac{\pi^2}{30}(g_* T_\sigma^4/3M_{pl}^2)}. \quad (\text{B1})$$

T_σ should be larger than BBN energy scale 10MeV. We also require that the curvaton decayed before the PBH creation, $T_\sigma > 10^5$ GeV(PBH-DM case) and $T_\sigma > 30$ MeV(LIGO-PBH case) in Eq.(12). T_R is conventionally assumed to 10^5 GeV $\sim 10^{14}$ GeV. Note that in our typical parametrization, $v^2\theta_i^2/(6M_{pl}^2) \sim 10^{-6}$ for both PBH-DM and LIGO-PBH cases.

Thus, $r = \mathcal{O}(0.1)$ in Table(I) requires the $(\frac{T_R}{T_\sigma}) \sim 10^5$. For example, with $T_R = 10^{12}$ GeV, the curvaton decay occurs at $T_\sigma \sim 10^7$ GeV. Both the DM-PBH and the LIGO-PBH scenario are available, but only for the limited parameter regions.

With typical curvaton decay parametrization $\Gamma_\sigma = (\kappa^2/16\pi)(m_\sigma^3/f^2)$, we can check the validity of our assumption $m_\phi > m_\sigma > \Gamma_R > \Gamma_\sigma$. Taking $T_\sigma \sim 10^7$ GeV, we get $\Gamma_\sigma \sim T_\sigma^2/M_{pl} \sim 10^{-2}$ GeV, $m_\sigma \sim (16\pi v^2\Gamma_\sigma/\kappa^2)^{1/3} \sim 10^{10}$ GeV. With $T_R = 10^{12}$ GeV and $\Gamma_R \sim T_R^2/M_{pl} \sim 10^6$ GeV, we get

$$m_\phi(\sim 10^{13} \text{GeV}) > m_\sigma(\sim 10^{10} \text{GeV}) > \Gamma_R(\sim 10^6 \text{GeV}) > \Gamma_\sigma(\sim 10^{-2} \text{GeV}). \quad (\text{B2})$$

-
- [1] B. P. Abbott *et al.* (Virgo, LIGO Scientific), *Phys. Rev. Lett.* **116**, 061102 (2016), arXiv:1602.03837 [gr-qc].
[2] B. P. Abbott *et al.* (Virgo, LIGO Scientific), *Phys. Rev. X* **6**, 041015 (2016), arXiv:1606.04856 [gr-qc].
[3] B. P. Abbott *et al.* (Virgo, LIGO Scientific), *Phys. Rev. Lett.* **116**, 241103 (2016), arXiv:1606.04855 [gr-qc].

- [4] B. P. Abbott *et al.* (VIRGO, LIGO Scientific), *Phys. Rev. Lett.* **118**, 221101 (2017), arXiv:1706.01812 [gr-qc].
- [5] B. P. Abbott *et al.* (Virgo, LIGO Scientific), *Astrophys. J.* **851**, L35 (2017), arXiv:1711.05578 [astro-ph.HE].
- [6] B. P. Abbott *et al.* (Virgo, LIGO Scientific), *Phys. Rev. Lett.* **119**, 141101 (2017), arXiv:1709.09660 [gr-qc].
- [7] K. Belczynski, T. Bulik, C. L. Fryer, A. Ruiter, J. S. Vink, and J. R. Hurley, *Astrophys. J.* **714**, 1217 (2010), arXiv:0904.2784 [astro-ph.SR].
- [8] M. Spera, M. Mapelli, and A. Bressan, *Mon. Not. Roy. Astron. Soc.* **451**, 4086 (2015), arXiv:1505.05201 [astro-ph.SR].
- [9] B. P. Abbott *et al.* (Virgo, LIGO Scientific), *Astrophys. J.* **818**, L22 (2016), arXiv:1602.03846 [astro-ph.HE].
- [10] T. Kinugawa, K. Inayoshi, K. Hotokezaka, D. Nakauchi, and T. Nakamura, *Mon. Not. Roy. Astron. Soc.* **442**, 2963 (2014), arXiv:1402.6672 [astro-ph.HE].
- [11] S. Bird, I. Cholis, J. B. Muñoz, Y. Ali-Haïmoud, M. Kamionkowski, E. D. Kovetz, A. Raccanelli, and A. G. Riess, *Phys. Rev. Lett.* **116**, 201301 (2016), arXiv:1603.00464 [astro-ph.CO].
- [12] S. Clesse and J. García-Bellido, *Phys. Dark Univ.* **15**, 142 (2017), arXiv:1603.05234 [astro-ph.CO].
- [13] M. Sasaki, T. Suyama, T. Tanaka, and S. Yokoyama, *Phys. Rev. Lett.* **117**, 061101 (2016), arXiv:1603.08338 [astro-ph.CO].
- [14] Yu. N. Eroshenko, (2016), arXiv:1604.04932 [astro-ph.CO].
- [15] B. Carr, F. Kuhnel, and M. Sandstad, *Phys. Rev. D* **94**, 083504 (2016), arXiv:1607.06077 [astro-ph.CO].
- [16] S. Hawking, *Mon. Not. Roy. Astron. Soc.* **152**, 75 (1971).
- [17] B. J. Carr and S. W. Hawking, *Mon. Not. Roy. Astron. Soc.* **168**, 399 (1974).
- [18] B. J. Carr, *Astrophys. J.* **201**, 1 (1975).
- [19] R. A. Allsman *et al.* (Macho), *Astrophys. J.* **550**, L169 (2001), arXiv:astro-ph/0011506 [astro-ph].
- [20] P. Tisserand *et al.* (EROS-2), *Astron. Astrophys.* **469**, 387 (2007), arXiv:astro-ph/0607207 [astro-ph].
- [21] L. Wyrzykowski *et al.*, *Mon. Not. Roy. Astron. Soc.* **416**, 2949 (2011), arXiv:1106.2925 [astro-ph.GA].
- [22] H. Niikura, M. Takada, N. Yasuda, R. H. Lupton, T. Sumi, S. More, A. More, M. Oguri, and M. Chiba, (2017), arXiv:1701.02151 [astro-ph.CO].
- [23] E. Bugaev and P. Klimai, *Phys. Rev. D* **85**, 103504 (2012), arXiv:1112.5601 [astro-ph.CO].
- [24] K. Inomata, M. Kawasaki, K. Mukaida, and T. T. Yanagida, *Phys. Rev. D* **97**, 043514 (2018), arXiv:1711.06129 [astro-ph.CO].
- [25] K. Kohri, C.-M. Lin, and T. Matsuda, *Phys. Rev. D* **87**, 103527 (2013), arXiv:1211.2371 [hep-ph].
- [26] K. Ando, K. Inomata, M. Kawasaki, K. Mukaida, and T. T. Yanagida, (2017), arXiv:1711.08956 [astro-ph.CO].
- [27] M. Kawasaki, N. Kitajima, and T. T. Yanagida, *Phys. Rev. D* **87**, 063519 (2013), arXiv:1207.2550 [hep-ph].
- [28] M. Kawasaki, N. Kitajima, and S. Yokoyama, *JCAP* **1308**, 042 (2013), arXiv:1305.4464 [astro-ph.CO].
- [29] M. Kawasaki and Y. Tada, *JCAP* **1608**, 041 (2016), arXiv:1512.03515 [astro-ph.CO].
- [30] T. Harada, C.-M. Yoo, and K. Kohri, *Phys. Rev. D* **88**, 084051 (2013), [Erratum: *Phys. Rev. D* 89, no. 2, 029903 (2014)], arXiv:1309.4201 [astro-ph.CO].
- [31] K. Ando, K. Inomata, and M. Kawasaki, (2018), arXiv:1802.06393 [astro-ph.CO].
- [32] C. T. Byrnes, E. J. Copeland, and A. M. Green, *Phys. Rev. D* **86**, 043512 (2012), arXiv:1206.4188 [astro-ph.CO].
- [33] S. Young and C. T. Byrnes, *JCAP* **1308**, 052 (2013), arXiv:1307.4995 [astro-ph.CO].
- [34] R. Saito and J. Yokoyama, *Prog. Theor. Phys.* **123**, 867 (2010), [Erratum: *Prog. Theor. Phys.* 126, 351 (2011)], arXiv:0912.5317 [astro-ph.CO].
- [35] K. Inomata, M. Kawasaki, K. Mukaida, Y. Tada, and T. T. Yanagida, *Phys. Rev. D* **95**, 123510 (2017), arXiv:1611.06130 [astro-ph.CO].
- [36] D. J. Fixsen, E. S. Cheng, J. M. Gales, J. C. Mather, R. A. Shafer, and E. L. Wright, *Astrophys. J.* **473**, 576 (1996), arXiv:astro-ph/9605054 [astro-ph].
- [37] J. Chluba, A. L. Erickcek, and I. Ben-Dayan, *The Astrophysical Journal* **758**, 76 (2012).
- [38] K. Inomata, M. Kawasaki, and Y. Tada, *Phys. Rev. D* **94**, 043527 (2016), arXiv:1605.04646 [astro-ph.CO].
- [39] E. Aver, K. A. Olive, and E. D. Skillman, *JCAP* **1507**, 011 (2015), arXiv:1503.08146 [astro-ph.CO].
- [40] H. C. Ohanian, *International Journal of Theoretical Physics* **9**, 425 (1974).
- [41] P. V. Bliokh and A. A. Minakov, *Astrophysics and Space Science* **34**, L7 (1975).
- [42] R. J. Bontz and M. P. Haugan, *Astrophysics and Space Science* **78**, 199 (1981).
- [43] Y. Ali-Haïmoud and M. Kamionkowski, *Phys. Rev. D* **95**, 043534 (2017), arXiv:1612.05644 [astro-ph.CO].
- [44] Y. Inoue and A. Kusenko, *JCAP* **1710**, 034 (2017), arXiv:1705.00791 [astro-ph.CO].
- [45] P. W. Graham, S. Rajendran, and J. Varela, *Phys. Rev. D* **92**, 063007 (2015), arXiv:1505.04444 [hep-ph].
- [46] L. Lentati *et al.*, *Mon. Not. Roy. Astron. Soc.* **453**, 2576 (2015), arXiv:1504.03692 [astro-ph.CO].
- [47] Z. Arzoumanian *et al.* (NANOGrav), *Astrophys. J.* **821**, 13 (2016), arXiv:1508.03024 [astro-ph.GA].
- [48] R. M. Shannon *et al.*, *Science* **349**, 1522 (2015), arXiv:1509.07320 [astro-ph.CO].
- [49] G. Janssen *et al.*, *Proceedings, Advancing Astrophysics with the Square Kilometre Array (AASKA14): Giardini Naxos, Italy, June 9–13, 2014*, PoS **AASKA14**, 037 (2015), arXiv:1501.00127 [astro-ph.IM].
- [50] C. J. Moore, R. H. Cole, and C. P. L. Berry, *Class. Quant. Grav.* **32**, 015014 (2015), arXiv:1408.0740 [gr-qc].